Estimates of Low-Frequency Sound Speed and Attenuation in a Surface Mud Layer Using Low-Order Modes

Lin Wan, Mohsen Badiey, David P. Knobles, Preston S. Wilson, and John A. Goff

***Abstract*—Whereas there have been numerous theoretical and experimental studies on the properties of marine granular sands, there are significantly fewer studies on sediments classified as muds. The validity of geoacoustic models for muddy sediments has not been successfully tested due to the lack of inverted low-frequency sound speed and attenuation values. The geoacoustic properties of a surface fine-grained mud layer, overlaying three sand transition layers, and a half-space basement within the New England Mud Patch, were studied using explosive signals from long-range along-shelf sound propagation tracks. The sound-speed profile of the mud layer in the low-frequency band (100–500 Hz) was estimated using acoustic normal mode characteristics including the mode shapes and the modal dispersion curves of low-order modes, which mainly propagated in the water column and the surface mud layer. The ambiguity of sound speed at the top of the mud layer and sound-speed gradient was approximately removed. It was found that the resultant sound-speed ratio at the water-sediment interface was close to unity and the sound-speed gradient was 1.8 1/s with a standard deviation of 1.0 1/s. The attenuation in the mud layer was inverted using the attenuation coefficient of the first mode extracted from explosive signals at three source locations. The estimated attenuation at 150 Hz had a mean of 0.006 dB/m and a standard deviation of 0.003 dB/m.**

***Index Terms*—Ambiguity removal, dimension reduction, geoacoustic inversion, low-frequency sound speed and attenuation, muddy sediment, normal mode, seabed characterization experiment (SBCEX).**

I. Introduction

GENERALLY, the ocean floor can be characterized by mean grain size or type (e.g., gravel, sand, and mud) [1]–[5]. In shallow water continental shelves, most of the ocean sediments range from sand to mud [2]. Whereas the physical mechanisms controlling sound propagation in marine granular sands have been studied theoretically and experimentally, far less attention has been paid to muds, which have more silt and clay content and smaller mean grain size than sandy sediment. Recently, there has been a growing interest in the acoustic properties (e.g., sound speed and attenuation) of muddy sediments in part because of their scientific complexity but also due to human kind's ever increasing activity in the ocean.

A shallow-water seabed characterization acoustic experiment (SBCEX 2017) [6], along with a series of environmental surveys, was conducted in a 30 km by 11 km area on the southern New England shelf. The experimental area, previously referred to as the New England Mud Patch [7], [8], has a surface fine-grained sediment layer composed of around 60% silt, 30% sand, and 10% clay [9]. This feature makes the Mud Patch a location for studying the geoacoustic properties of muddy sediments.

Direct measurements of sediment properties are expensive and spatially limited. They generally disturb the ambient sediment structure and can thus bias the sound-speed measurements. The small value of sound attenuation at low frequencies (e.g., below 600 Hz) precludes direct measurements, because the distances required to achieve detectability are at least hundreds or thousands of meters. In addition, direct measurements made at high frequencies (i.e., larger than 5 kHz) may have little physical relevance to trying to understand the low-frequency response of a sediment. Therefore, the inversion methods based on acoustic field measurements (i.e., acoustic remote sensing) have been exploited to estimate low-frequency sediment properties. These inversion techniques involve normal mode analysis [10]–[25], matched field processing [26]–[28], signal waveform matching [29]–[32], transmission loss [33], [34], spatial coherence of reverberation and propagation [23], [35], ambient noise correlation [36], [37], reflection coefficient [38], [39], Hankel transform [40], [41], and multipath arrival time [42].

The cost functions of the full-field inversion approaches (e.g., matched field processing) calculate the difference between measured acoustic field and forward model predictions, which usually include a high-dimensional parameter space to describe all the full-field features in the measured data. The difficulty that arises from this high dimensionality is the parameter ambiguity (e.g., seabed sound speed–attenuation coupling discussed in [43]). Dimension reduction can be achieved by two ways: first, using the prior knowledge from direct measurements as constraints or second, defining cost functions measuring the data-model misfit of a particular feature that depends only on the

Manuscript received October 29, 2018; revised March 16, 2019; accepted May 14, 2019. Date of publication August 2, 2019; date of current version January 13, 2020. This work was supported by the U.S. Navy Office of Naval Research, Ocean Acoustics Program (ONR322OA) via Grants N00014-18-1-2168, N00014-18-1-2140, N00014-16-C-3065, N00014-16-1-2775, and N00014-18-1-2438. *(Corresponding author: Lin Wan.)*

Associate Editor: D. Simons.

L. Wan and M. Badiey are with the University of Delaware, Newark, DE 19716 USA (e-mail: wan@udel.edu; badiey@udel.edu).

D. P. Knobles is with the Knobles Scientific and Analysis, LLC, Austin, TX 78755 USA, and also with the University of Delaware, Newark, DE 19716 USA (e-mail: dpknobles@kphysics.org).

P. S. Wilson is with the Department of Mechanical Engineering and Applied Research Laboratories, The University of Texas at Austin, Austin, TX 78713 USA (e-mail: pswilson@mail.utexas.edu).

J. A. Goff is with the Institute for Geophysics, The University of Texas at Austin, Austin, TX 78713 USA (e-mail: goff@ig.utexas.edu).

Digital Object Identifier 10.1109/JOE.2019.2923861

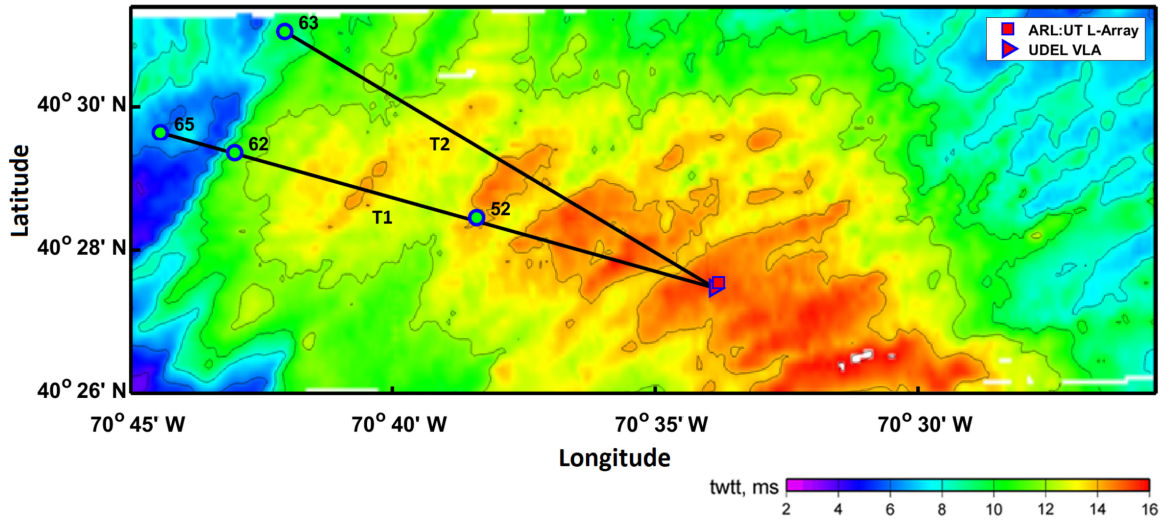

Fig. 1. Mud thickness map in terms of TWTT in units of milliseconds [46], [47]. 20 explosive charges, deployed at four firing stations (shown as dots) on two along-shelf tracks (T1 and T2), were utilized for estimating the sound speed and attenuation in mud. The signals were recorded at a sampling frequency of 9600 Hz by an L-shaped array (marked by a square).

subset of the parameter space. In this paper, we will first utilize the analyzed environmental data from SBCEX 2017 and the data from a subbottom profiler survey as constraints and, then, extract three modal characteristic features (i.e., modal arrival time, mode shape, and modal amplitude of low-order modes) to construct physics-based cost functions mainly depending on the geoacoustic properties of the surface mud layer. The sound-speed profile (SSP) and attenuation can be estimated by an exhaustive search of the parameter space with reduced dimensions.

The modal dispersion curve has been utilized to estimate the sea bottom properties at the site of SBCEX 2017 [24], [25]. In particular, the detailed structure of the Airy phase corresponding to the group speed minimum of low-order modes was observed using long-range explosive sound signals. A sensitivity analysis indicated that the Airy phase structure was mostly affected by the sound speed in the half-space basement [24]. The ambiguity of sound speed at the top of the mud layer and sound-speed gradient cannot be completely removed by using the low-frequency (10–80 Hz) modal dispersion curve with Airy phase structure [24]. In [25], high-order modes over the frequency band 20–440 Hz were resolved and estimated using a warping method and a combustive sound source signal at a range of 4.8 km along a range-dependent track. The inversion, using high-order modes, provided estimations of sound speed and density in the mud layer and deeper sediment layers as well as the basement.

In this paper, we focus on the low-order modes of explosive signals, which have propagated out to long ranges (up to 15.45 km), from along-shelf propagation tracks to estimate the sound speed and attenuation in the mud layer in the low-frequency band (100–500 Hz). The rationale of choosing this data set is explained as follows.

1) The estimation of a small value of low-frequency sound attenuation in mud requires a long propagation distance to achieve detectability.
2) The low-order modes are separated in the time domain at long ranges. Their modal amplitudes and arrival times could be simply extracted using appropriate source–receiver configurations [19]. This mode separation technique does not rely on advanced mode filtering methods [16], [21], [44]. Therefore, the uncertainty introduced by these methods is eliminated.
3) For a given frequency, low-order modes with small grazing angles will generally travel in shallower layers in the sediment than high-order modes with large grazing angles. Particularly, the characteristics of the first mode in the frequency band (100–500 Hz) are mainly determined by the geoacoustic properties of the surface mud layer. Thus, the dimension of the parameter space could be significantly reduced and the effect of the uncertainty from propagation in the deep sand transition layers and half-space basement might be minimized. The idea of using the dimension-reduced parameter space and the first-order modal arrivals has also been discussed in [32].
4) The presence of a well-mixed ocean as confirmed by environmental measurements largely mitigates uncertainties due to the water column. The use of nearly isobathic along-shelf propagation tracks further reduces the complexity of the shallow water waveguide. Assuming the sediment properties did not change as a function of range, we could treat these long-range tracks as weak range-dependent ones in part because of the small bathymetric variance (0.6 m), which was within 1% of the water depth. Given the change of layer thickness in the mud layer, the validity of the adiabatic approximation was justified for low-order modes using the criteria derived by Milder [45]. Therefore, the adiabatic approximation is utilized for this research.

The remainder of this paper is organized as follows. Section II describes the experimental configuration and analyzes the environmental measurements. Section III demonstrates the normal mode analysis of long-range explosive sound signals. Section IV presents the estimates of SSP in the surface mud layer using the mode shape and the modal dispersion curve. The ambiguity of sound speed at the top of the mud layer and sound-speed gradient

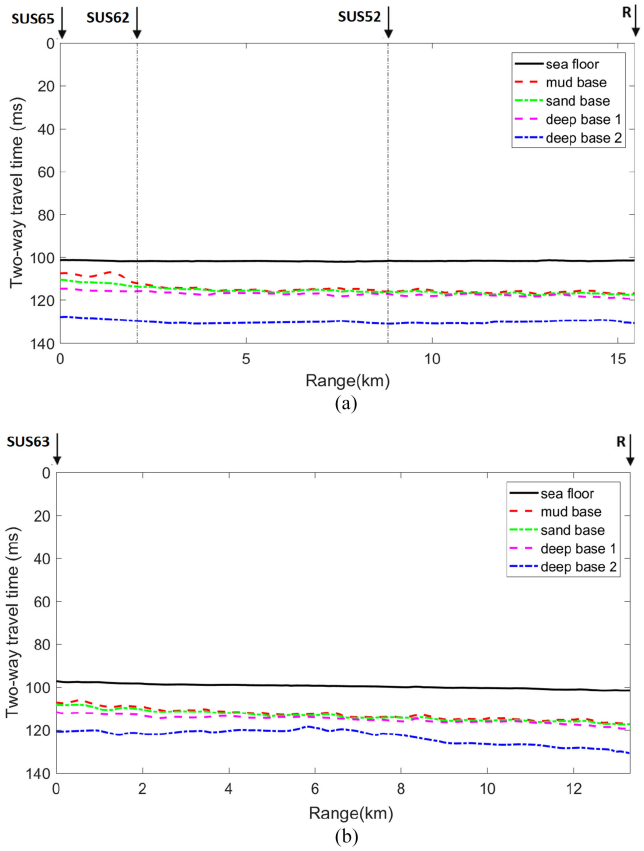

Fig. 2. Sediment layer structure along (a) track T1 and (b) track T2 [46], [47].

is examined and approximately removed. In Section V, attenuation in the mud layer is inverted using the modal attenuation coefficient extracted from modal amplitudes at three ranges. The uncertainty of estimated mud attenuation due to modal amplitude measurement, source level, and source depth is evaluated. Finally, concluding remarks appear in Section VI.

II. Experimental Configuration and Environmental Measurements

The sea bottom at the SBCEX site has been extensively surveyed in a series of experiments (i.e., a chirp sonar survey in summer 2015 [46], [47], a vibracore survey and a piston survey in 2016 [9], [48]). Fig. 1 is the mud thickness map in terms of two-way travel time (TWTT) in units of milliseconds (ms), which was obtained using the 2015 survey data [46], [47]. The analysis of the chirp sonar survey data suggests that this area can be approximated by a surface mud layer overlaying three sand transition layers and a half-space basement. Fig. 2 presents the sediment layering structure of two along-shelf tracks (T1 and T2, shown as two straight lines in Fig. 1).

The water temperature was monitored using the ships' casts of conductivity, temperature, and depth (CTD) and the environmental sensors attached to vertical line arrays (VLAs) during both the main experiment in 2017 and the survey in 2015. Fig. 3(a) shows the water column SSP as a function of geotime (from 5:00 to 11:00 Z on March 18, 2017) at the center of the experimental area (40.4572° N, 70.5643° W), determined using the environmental data from a VLA deployed by the University of Delaware (UDEL VLA, marked by a triangle in Fig. 1). The solid line and the dashed line shown in Fig. 3(b) represent the SSPs measured in summer 2015 and in spring 2017, respectively. Whereas the water column had a strong thermocline in summer, it was well mixed (i.e., almost isothermal) in the spring time when the acoustic measurements were made. It should be noted that the 2017 spring SSP is applied in the acoustic data analysis and the 2015 summer SSP is used to convert the 2015 TWTT to water depth. From March 17 to 18, 2017, three CTD casts by two research vessels, *Neil Armstrong* (NA) and *Endeavor* (EN), were performed in the experimental area. Table I summarizes these measurements and lists the maximum temperature difference between these CTD casts and the measurements by the UDEL VLA. The temperature difference was no greater than 0.7 °C.

III. Normal Mode Analysis of Explosive Sounds

During the main SBCEX experiment in 2017, both narrowband and broadband acoustic sources were deployed at various ranges, depths, and azimuths. In this paper, 20 explosive charges with 31-g TNT equivalent, also known as Mk-64 signals underwater sound (SUS), were utilized for estimating the sound speed and attenuation in mud. They were deployed at four firing stations on two along-shelf tracks. The four firing stations, five shots per station, are marked as four dots (SUS52, SUS62, SUS63, and SUS65) in Fig. 1 and are also indicated by vertical lines in Fig. 2. Table II summarizes the information for these SUS charges. The signals of these 20 explosions with a source depth of 18.3 m were recorded at a sampling frequency of 9.6 kHz by an L-shaped array (shown as a square in Fig. 1) deployed by the Applied Research Laboratories of the University of Texas at Austin (ARL:UT). The VLA portion, located approximately 172 m away from the UDEL VLA, had 14 hydrophones with an element-spacing of 4.37 m. The horizontal line array (HLA) portion was positioned on the seafloor.

Normal mode characteristics have been applied in geoacoustic inversion since the 1970s–1980s [10]–[13]. Successful inversions are dependent on accurate extractions of modal arrival time, mode shape, and modal amplitude from broadband acoustic signals. As signal processing techniques advance, state-of-the-art time-frequency analysis tools and mode filtering methods have been developed for the separation of normal modes [15]–[25]. On the other hand, most of these methods increase the complexity of the modal extraction and might introduce uncertainties due to certain assumptions used in data processing. For instance, the assumption of orthogonality between different mode shapes without including the unmeasured pressure field in the sediment may cause a bias in the extraction of high-order modes, which have nonnegligible energy contained in the sea bottom [44]. Here, we simplify the mode filtering process by choosing long-range propagation tracks during SBCEX 2017. Especially for the shots at the SUS65 station (15.45 km), the first modal arrivals were easily separated in the time domain from other modes by applying a bandpass filter with a center frequency of 150 Hz.

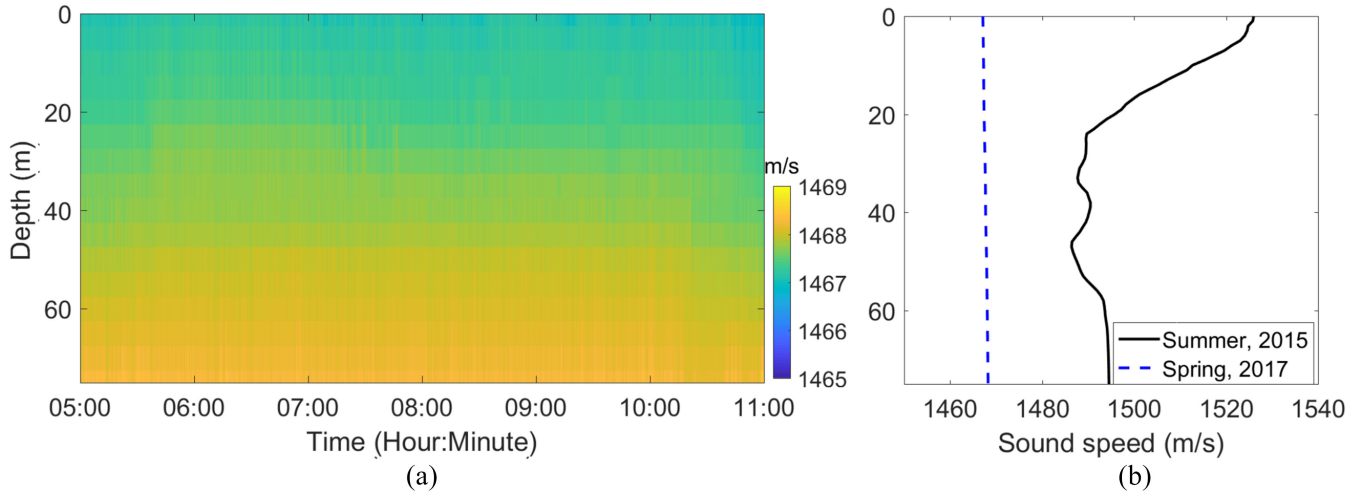

Fig. 3. (a) Water column sound speed at the UDEL VLA during the deployment of SUS charges in the spring of 2017 (from 5:00 to 11:00 Z, March 18, 2017). (b) SSP comparison between summer 2015 (04:35 Z, July 27, 2015) and spring 2017 [averaged result from (a)].

TABLE I
CTD CASTS FROM RESEARCH VESSELS, NA AND EN, AND TEMPERATURE DIFFERENCE COMPARED WITH UDEL ARRAY LOCATION

Cast #	Location (Lon, Lat)	Time (Z)	Distance (km)	ΔT° C
NA1	70.580° W, 40.446° N	23:48, March 17, 2017	2.0	0.07
NA2	70.452° W, 40.499° N	13:59, March 18, 2017	10.4	0.70
EN1	70.629° W, 40.489° N	20:54, March 18, 2017	6.4	0.40

Fig. 4(a) shows the filtered mode one (solid curves) and its envelope (dashed curves) as a function of hydrophone depth, which was measured by 14 depth sensors mounted on the VLA. The result at the depth of 75 m was from the seafloor positioned HLA hydrophone, which was 37.3 m away from the VLA. Its arrival time value was shifted to compensate for the distance offset. The filtered signals have been normalized and shifted for easy graphical viewing. The amplitude value of mode one was measured at the peak of its envelope. Fig. 4(b) demonstrates the normalized modal amplitudes for all five shots at the SUS65 station.

At higher frequencies, the arrival time difference between low-order modes generally becomes smaller, thus mode filtering of low-order modes is more challenging. A mode separation technique was utilized here to obtain the modal arrival time and amplitude at a node of its neighboring mode [19]. We use the first shot at the SUS65 station as an example to explain our data processing. Since the second mode was close to its node at the depth of the eighth hydrophone (43.8 m) at 350 Hz, the signal received by this channel was employed to get the modal arrival time and amplitude of the first and third modes. Fig. 5 shows the signals (from top to bottom) filtered by the bandpass filters with a bandwidth of 100 Hz and center frequencies of 450, 350, and 150 Hz, respectively. The result in the band 200–300 Hz is not presented due to the existence of electronic noise in this band, which was caused by a ground fault within the array recording system. The shock waves of the first and third modes are identified in Fig. 5. Their arrival times, corresponding to the peak values of the envelops, are marked as squares. The bubble pulse (BP) arrivals of the first mode can also be recognized using the measured first BP period (i.e., 41.6 ms) [49]. In Section IV, the extracted mode shape and modal arrival time shown in Figs. 4 and 5 are utilized to estimate the SSP in the surface mud layer.

TABLE II
INFORMATION FOR SUS CHARGES

Station	Location (Lon, Lat)	Range	Time (Z)	Track
SUS65	70.740° W, 40.494° N	15.45 km	10:34, March 18, 2017	T1
SUS62	70.716° W, 40.491° N	13.38 km	10:00, March 18, 2017	T1
SUS52	70.639° W, 40.474° N	6.63 km	05:27, March 18, 2017	T1
SUS63	70.701° W, 40.518° N	13.33 km	09:36, March 18, 2017	T2

IV. ESTIMATES OF SSP IN MUD LAYER USING THE MODE SHAPE AND THE MODAL DISPERSION CURVE

In this section, the two-stage inversion process, including mode shape based inversion in Section IV-A and modal dispersion based inversion in Section IV-B, will be utilized to estimate sound speed (c_1) at the top of the mud layer and speed gradient (s_1) in the entire mud layer. In the first stage, the mode shape is utilized to define the first cost function calculating the difference between the modeled and measured mode shape. A strong coupling between c_1 and s_1 is obtained using an exhaustive search. In the second stage, the modal dispersion characteristics are applied in constructing the second cost function to remove the ambiguity between c_1 and s_1 from the first stage.

A. Mode-Shape-Based Inversion

The mode shape has been successfully applied in the estimation of sound speed in half-space bottom environments [16],

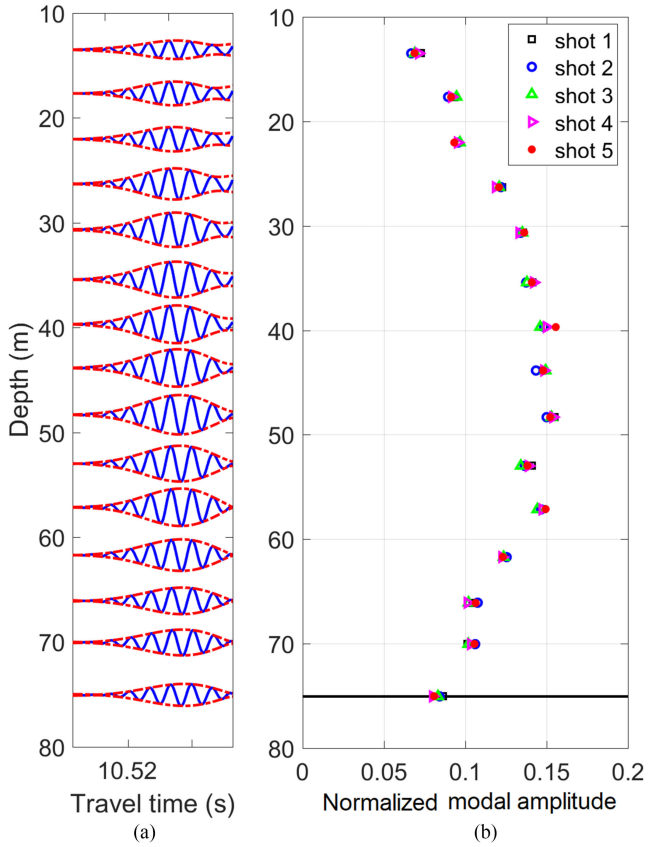

Fig. 4. Extraction of the first mode at 150 Hz. (a) Filtered mode one (solid curves) and its envelope (dashed curves) as a function of hydrophone depth. The filtered signals have been normalized and shifted for easy graphical viewing. (b) Normalized modal amplitudes of the first mode for all five shots at the SUS65 station.

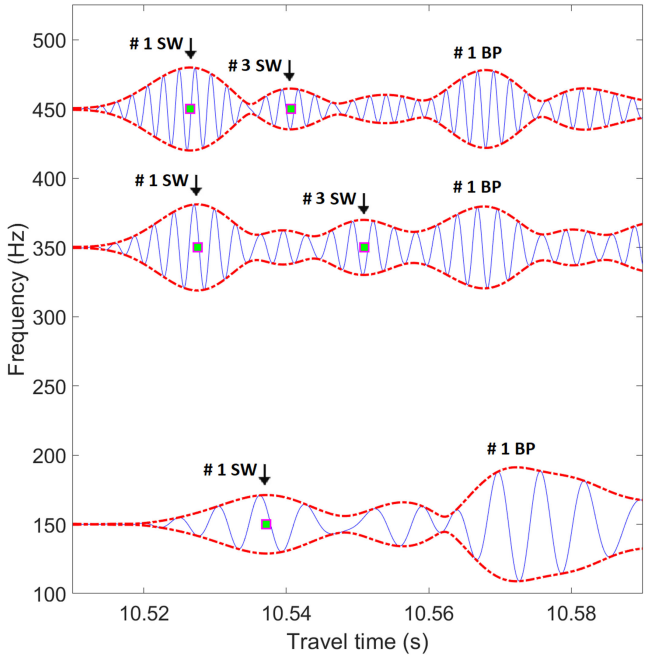

Fig. 5. Signals (from top to bottom) filtered by the bandpass filters with a bandwidth of 100 Hz and center frequencies of 450, 350, and 150 Hz, respectively. The result in the band 200–300 Hz is not presented due to electronic noise. The SWs of the first and third modes are identified. Their arrival times, corresponding to the peak values of the envelops, are marked as squares.

[19]. Since the first mode at 150 Hz mainly traveled in the water column and the surface mud layer, it was not too sensitive to the geoacoustic parameters in the three transition layers and the half-space basement. The cost function, calculating the difference between modeled and measured mode shape, is defined as

$$E_1(c_1, s_1) = \sqrt{\frac{1}{N_{\text{phone}}} \sum_{j=1}^{N_{\text{phone}}} (\psi_1(z_j) - \hat{\psi}_1(z_j))^2} \qquad (1)$$

where c_1 is the unknown sound speed at the top of the mud layer; s_1 is the unknown sound-speed gradient. N_{phone} is the number of hydrophones; $\hat{\psi}_1(z_j)$ is the normalized modal amplitude from measurements, shown in Fig. 4(b), at the depth of the jth hydrophone; $\psi_1(z_j)$ is the calculated mode shape obtained using the normal mode model, KRAKEN [50].

The input geoacoustic parameter values for this calculation are listed in Table III. It is noted that the values for sound speed in the three sand transition layers and the half-space basement were estimated from the geoacoustic inversion using modal dispersion curves with Airy phase structures in the frequency range of 10–80 Hz [24]. The value for the density in mud was inferred from piston core data collected close to the VLA [48]. The environmental data (e.g., water temperature, salinity, and water depth) measured at the time of acoustic transmissions were fed to the normal mode simulation model. The TWTT in units of milliseconds, from bottom surveys [46], [47], was used as a constraint to determine the mud layer thickness (H_{mud}) through [24]

$$H_{\text{mud}} = c_1 \Big/ \left[\frac{2000}{\text{TWTT}} - \frac{s_1}{2} \right]. \qquad (2)$$

An exhaustive search was performed to find the inverted value for c_1 and s_1, corresponding to the minimum of the cost function (1). The search band for s_1 was from -9 to 13 1/s with a step size of 0.5 1/s. For c_1, the cost function was calculated every 1 m/s between 1430 and 1510 m/s. After 3645 (i.e., 45×81) model runs, the value of E_1 as a function of c_1 and s_1 is shown in Fig. 6. A strong coupling between c_1 and s_1 is observed. For further analysis, we chose three pairs of c_1 and s_1 with small data-model mismatch and marked them as circles in Fig. 6. Table IV lists the values of c_1 and s_1 for these three cases (i.e., no sound-speed gradient, positive gradient, and negative gradient). Fig. 7 demonstrates their (a) SSPs, (b) mode shape of mode 1 and (c) mode shape of mode 3 at 150 Hz. The SSPs in sand transition layers and below are not shown.

In Fig. 7(b), the normalized modal amplitudes of the first mode from measurements (black squares in the water column) are in good agreement with the calculated results for all three cases, which represent the ambiguity between c_1 and s_1. The small value of the normalized modal amplitudes below the mud layer indicates that the first mode at 150 Hz mainly propagated in the water column and the surface mud layer. Thus, it was not

TABLE III
GEOACOUSTIC PARAMETERS FOR INVERSION

	Density (kg/m^3)	Top sound speed (m/s)	Speed gradient $(1/s)$
Mud layer	1665.1	c_1	s_1
Sand layer	1800.0	1614.2	0
Deep layer 1	1900.0	1725.5	0
Deep layer 2	1900.0	1778.0	0
Basement	2100.0	1782.0	0

sensitive to the geoacoustic parameters in the sand transition layers and below.

The variation of the mode shapes in the mud layer is presented in Fig. 7(b) and (c) for all three cases. The modal arrival time reflecting this discrepancy can be used to remove the ambiguity between c_1 and s_1 as shown in Section IV-B.

B. Modal-Dispersion-Based Inversion

In normal mode theory, the group speed of the *n*th mode V_n, at a given frequency f, satisfies [12], [51]

$$\frac{1}{V_n(f)} = \frac{2\pi f}{k_n(f)N_n}\int_0^\infty \frac{\rho(z)}{c^2(z)}|U_n(z,f)|^2 dz \tag{3}$$

where k_n is the horizontal wave number; z is the depth down from the sea surface; ρ and c are the density and sound speed, respectively; U_n is the mode eigenfunction; N_n is the normalization factor of the *n*th mode and it can be defined by [10], [12]

$$N_n = \int_0^\infty \rho(z)|U_n(z,f)|^2 dz. \tag{4}$$

Then, the dispersive modal arrival time of the *n*th mode T_n, obtained by substituting the normalized modal amplitude, $\psi_n(z,f)$, into (3) and multiplying a range r on both sides of (3), can be written as

$$T_n(f) = \frac{2\pi f r}{k_n(f)}\int_0^\infty \frac{\rho(z)}{c^2(z)}|\psi_n(z,f)|^2 dz. \tag{5}$$

In a shallow water waveguide with a mud sediment layer overlaying sand transition layers and a half-space basement, the integral in (5) becomes

$$\begin{aligned}
&\int_0^\infty \frac{\rho(z)}{c^2(z)}|\psi_n(z,f)|^2 dz \\
&= \int_0^{H_w} \frac{\rho_w(z)}{c_w^2(z)}|\psi_n(z,f)|^2 dz \\
&\quad + \int_{H_w}^{H_w+H_{\text{mud}}} \frac{\rho_{\text{mud}}(z)}{\left(c_1 + s_1(z-H_w)\right)^2}|\psi_n(z,f)|^2 dz \\
&\quad + \int_{H_w+H_{\text{mud}}}^\infty \frac{\rho_b(z)}{c_b^2(z)}|\psi_n(z,f)|^2 dz
\end{aligned} \tag{6}$$

where H_w is the water depth; c_w and c_b are the sound speed in water and the layers below mud, respectively; ρ_w, ρ_{mud}, and ρ_b are the densities in water, the mud layer, and the layers below mud, respectively.

For the three cases shown in Fig. 7, the values of each term on the right side of (6) were calculated. Although the first integral's interval (H_w) was over seven times larger than the interval of the second term (H_{mud}), the difference in the values of the first term for the three cases was close to that of the second term due to the almost identical mode shapes ψ_n in the water column. They were of the order of 8×10^{-9}(s/m)^2. The variation in the values of the third term, depending on the properties in the layers below mud, was only 5% of 8×10^{-9}(s/m)^2 and negligible, because the value of the normalized modal amplitudes ψ_n was small in these layers. Therefore, the difference of modal arrival time for the three cases was dependent on the discrepancy of the mud properties as shown in the second term. Furthermore, the ambiguity between c_1 and s_1, represented by these three cases, could be removed by the cost function (7) calculating the difference between their simulated modal arrival times and the measured data demonstrated in Fig. 5

$$\begin{aligned}
&E_2(c_1, s_1) \\
&= \sqrt{\frac{1}{4}\sum_{j=2}^{3}\left[\left(\Delta T_1(f_j) - \Delta\hat{T}_1(f_j)\right)^2 + \left(\Delta T_3(f_j) - \Delta\hat{T}_3(f_j)\right)^2\right]}
\end{aligned} \tag{7}$$

where $f_j = 150$, 350, 450 Hz for $j = 1$, 2, 3. The arrival time of the first mode at 150 Hz, $T_1(f_1)$, is used as the reference

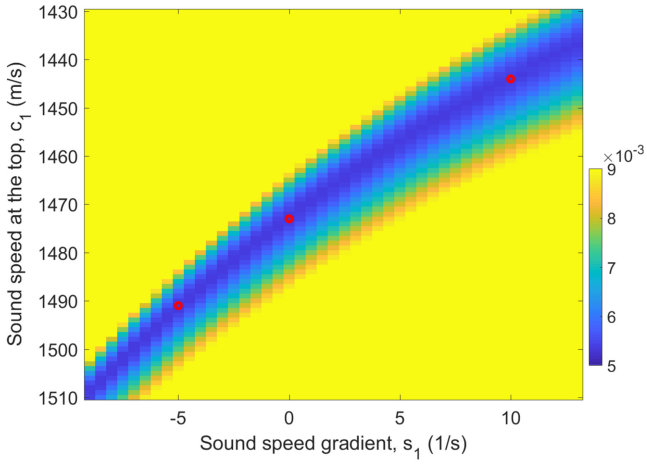

Fig. 6. Exhaustive search for sound speed at the top of the mud layer (c_1) and sound-speed gradient (s_1). A strong coupling between c_1 and s_1 is observed. Three pairs of c_1 and s_1 with small data-model mismatch are marked as circles.

TABLE IV
THREE CASES FOR COMPARISON

	c_1 (m/s)	s_1 $(1/s)$
Case 1	1473	0
Case 2	1444	10
Case 3	1491	-5

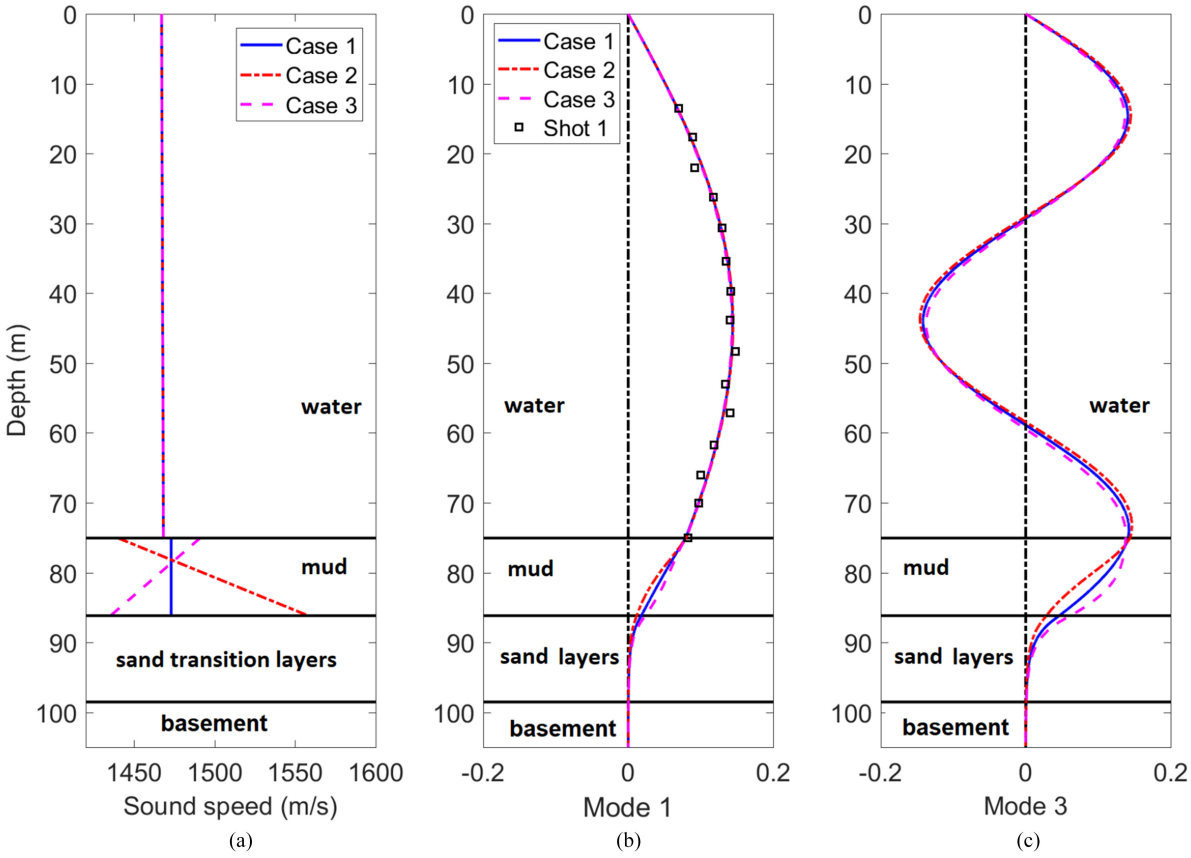

Fig. 7. (a) SSPs for three cases. (b) Comparison of calculated mode 1 with data at 150 Hz. (c) Mode shape comparison of mode 3 at 150 Hz.

time, thus $\Delta T_n(f_j) = T_n(f_j) - T_1(f_1)$. The parameters with and without the symbol hat $\hat{}$ are the measured and calculated results, respectively.

The travel time $T_n(f_j)$ was calculated in the same manner as in [24]. The 45 pairs of c_1 and s_1, corresponding to the minimum value of E_1 for each s_1 in the aforementioned exhaustive search (along the valley in Fig. 6), were utilized as inputs to the normal mode model. The value of E_2 as a function of c_1 and s_1 are illustrated in Fig. 8(a) and (b), respectively. For this example signal, s_1 and c_1 were estimated to be 0.5 1/s and 1471.0 m/s, respectively.

In Fig. 9, the calculated dispersion curves based on the parameter values of the three cases are plotted on top of the measured ones presented in Fig. 5. The comparison shows that the mismatch of the dispersion curves disqualified the second and third cases. The set of parameter values in the first case, close to the estimated values, provided a better fit to the extracted data.

For the five shots deployed at the SUS65 station, the estimated s_1 had a mean of 1.3 1/s and a standard deviation of 0.6 1/s. The estimated c_1 was 1468.8 $\pm$ 1.5 m/s and the mean sound-speed ratio at the water-sediment interface (i.e., c_1/c_w) was 1.0004. Besides the shots at the SUS65 station on the T1 track, the estimation process for c_1 and s_1 was also applied in the five shots deployed at the SUS63 station having the longest propagation distance on the T2 track. The resulting s_1 was 2.2 $\pm$ 1.2 1/s. The inverted c_1 had a mean of 1464.8 m/s and a standard deviation of 2.7 m/s and the mean sound-speed ratio was 0.9976. The value from both stations suggest that there was no very strong sound-speed gradient in the surface mud layer and the sound-speed ratio was close to unity. It is noticed from (3)–(5) that the modal travel time depends on the modal group speed, which is a range-averaged quantity along a range-dependent sound propagation track [24]. The small difference of estimated parameter values between T1 and T2 indicates that the sediment properties along these two tracks could be similar.

V. Estimates of Attenuation in Mud Layer Using the Modal Amplitude

The normal mode attenuation coefficient of the *n*th mode can be expressed by [10], [12], [51]

$$\begin{aligned}\beta_n(f) = {} & \frac{2\pi f}{k_n(f)} \int_0^{H_w} \frac{\alpha_w(z,f)\rho_w(z)}{c_w(z)} |\psi_n(z,f)|^2 dz \\ & + \frac{2\pi f}{k_n(f)} \int_{H_w}^{H_w+H_{\text{mud}}} \frac{\alpha_{\text{mud}}(z,f)\rho_{\text{mud}}(z)}{(c_1 + s_1(z-H_w))} |\psi_n(z,f)|^2 dz \\ & + \frac{2\pi f}{k_n(f)} \int_{H_w+H_{\text{mud}}}^{\infty} \frac{\alpha_b(z,f)\rho_b(z)}{c_b(z)} |\psi_n(z,f)|^2 dz \end{aligned} \quad (8)$$

where α_w, α_{mud}, and α_b are the attenuations in the water, the mud layer, and the layers below mud, respectively. According to the work in [43], $\alpha_b = (0.37 \pm 0.01)\ f^{1.80\pm0.02}$ dB/m, f is in units of kilohertz. The attenuation in water, α_w, can be calculated using the formula in [52]. Particularly, $\alpha_w = 0.003$ dB/km at 150 Hz. If we substitute the inverted values of c_1 and s_1 in (8), then $\alpha_{\text{mud}}(f)$ becomes the only unknown parameter for $\beta_n(f)$

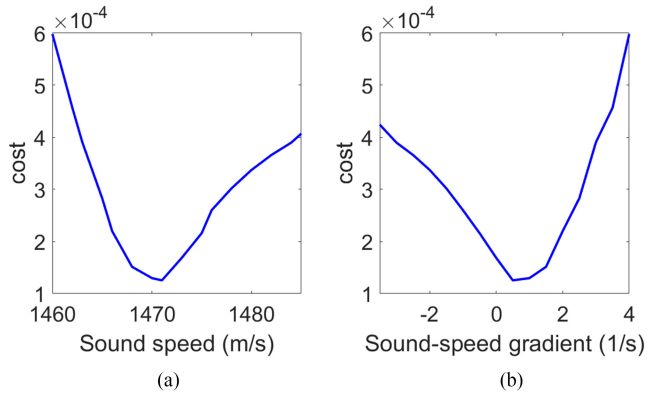

Fig. 8. (a) Value of E_2 as a function of c_1. (b) Value of E_2 as a function of s_1.

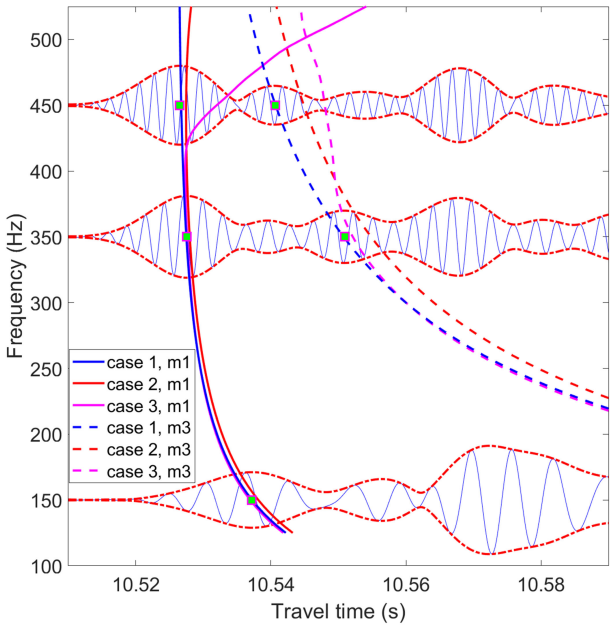

Fig. 9. Data-model comparison of the first (m1) and third (m3) modal arrival times for the three cases.

and it can be estimated by minimizing the difference between measured and modeled modal attenuation coefficient as shown in (9). Here, we assume that $\alpha_{\text{mud}}(f)$ is not depth dependent

$$E_3(\alpha_{\text{mud}}(f)) = |\beta_1(f) - \hat{\beta}_1(f)|. \tag{9}$$

The pressure amplitude of the *n*th mode (expressed in decibels and corrected for cylindrical spreading) can be described by [12]

$$\begin{aligned} &20\log|p_n(r,z,f)| + 10\log r \\ &\quad = -(20\log e)\beta_n(f)r + \text{SL}(f) \\ &\qquad + 20\log|\psi_n(z_0,f)| + 20\log|\psi_n(z,f)| + B \end{aligned} \tag{10}$$

where $p_n(r,z,f)$ is the pressure amplitude of the *n*th mode and it is proportional to $\psi_n(z,f)$; SL is the source level in decibels; z_0 is the source depth; B is a function of water depth and pulse length.

Along the T1 track, the experimental attenuation coefficient of the first mode ($\hat{\beta}_1$) at 150 Hz was obtained from the measurements of its pressure amplitude at three stations (i.e., SUS65, SUS62, and SUS52). Fig. 10 demonstrates the extracted pressure amplitude of the first mode (expressed in $20\log|p_1(r,z)| + 10\log r$) from the eighth hydrophone of the VLA as a function of range. At each range, there are five dots corresponding to five shots deployed at each station and received by the eighth hydrophone. If the source level, source depth, and receiver depth are held constant (i.e., $\text{SL}(f) + 20\log|\psi_1(z_0,f)| + 20\log|\psi_n(z,f)| + B$ is constant), the least-squares fit to the pressure amplitudes at these stations yielded a straight line with a slope of m and a vertical axis intercept of q, which satisfy

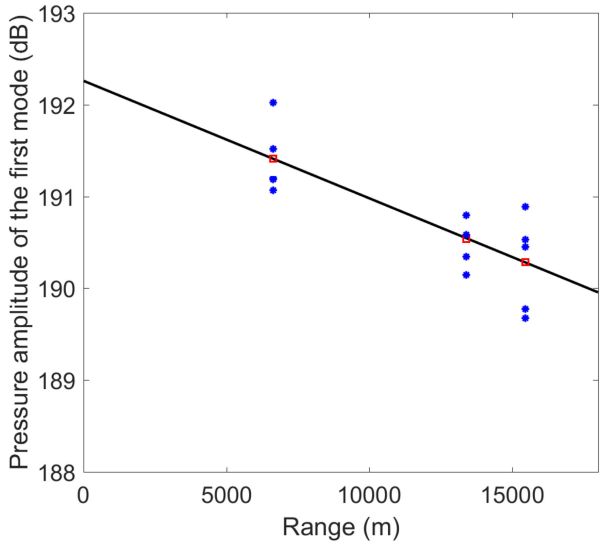

Fig. 10. Attenuation of the first normal mode at 150 Hz corrected for cylindrical spreading.

$$m = -(20\log e)\hat{\beta}_1 \tag{11}$$

and

$$q = \text{SL} + 20\log|\psi_1(z_0)| + 20\log|\psi_1(z)| + B. \tag{12}$$

Using the averaged first modal amplitudes (marked as squares in Fig. 10), we obtained the slope $m = -0.1280 \times 10^{-3}$ dB/m, then $\hat{\beta}_1 = 1.4737 \times 10^{-5}$ dB/m. By minimizing the difference between $\hat{\beta}_1$ and β_1, the estimated α_{mud} at 150 Hz was 0.006 dB/m.

It is noticed from Figs. 9 and 10 that, the uncertainty from the modal pressure amplitude measurement will pass to the estimation of mud attenuation. Using the 15 shots at these three stations (i.e., five shots per station), we quantified the uncertainty of the attenuation estimation and obtained the frequentist statistics as follows. According to (9)–(12), if we select one shot at each of these three stations (i.e., one dot at each range shown in Fig. 10), the least-squares fit to the three selected dots produces one straight line with one slope. Therefore, one attenuation estimate corresponding to the three shots can be made. There are 125 different combinations of shot selections (i.e., 5 selections at SUS65 × 5 at SUS62 × 5 at SUS52), which result in 125 attenuation estimates with a mean of 0.006 dB/m and a standard deviation of 0.003 dB/m.

The inverted mud attenuation (0.006 dB/m at 150 Hz) is smaller than that in sand (0.012 dB/m at 150 Hz [43]). Here,

we examine the uncertainty of mud attenuation due to the different assumed values of sand attenuation in the deeper layers by taking the upper (0.013 dB/m) and lower (0.011 dB/m) bound at 150 Hz for the sand attenuation and computing the corresponding mud attenuations. The variation of the resulting mud attenuations at 150 Hz is less than 2.3×10^{-5} dB/m, which is much smaller than the uncertainty (0.003 dB/m) caused by the modal amplitude measurement.

The variability of source level and source depth associated with the SUS charges deployed in SBCEX 2017 has been analyzed. The source level had a mean of 205.4 dB and a standard deviation of 0.9 dB in the frequency band with a center frequency of 150 Hz and a bandwidth of 100 Hz. The source depth, obtained from the bubble period analysis, was about 18.4 ± 1.1 m [49]. The effect of this variability on the attenuation inversion can be evaluated using the relationship shown in (13) between the variance of slope (σ_m^2) and intercept (σ_q^2) from a least-squares fit [53]

$$\sigma_m^2 = \sigma_q^2 \frac{N_{\text{shot}}}{\sum_{j=1}^{N_{\text{shot}}} r_j^2} \tag{13}$$

where N_{shot} is the number of shots (i.e., 15) and r_j is the range for the *j*th shot.

If the uncertainties from the last two terms of the right-hand side of (12) are negligible, the uncertainty of intercept is dependent on the variability of source level and source depth. Based on the propagation of uncertainty and by (11) and (12), (13) becomes

$$(20 \log e)^2 \sigma_{\beta_1}^2 = \left[\sigma_{\text{SL}}^2 + \left(\frac{20}{\ln(10)\psi_1(z_0)} \right)^2 \sigma_{\psi_1(z_0)}^2 \right] \frac{N_{\text{shot}}}{\sum_{j=1}^{N_{\text{shot}}} r_j^2} \tag{14}$$

where σ_{SL}^2 and $\sigma_{\beta_1}^2$ are the variance of source level and modal attenuation coefficient of the first mode, respectively; $\sigma_{\psi_1(z_0)}^2$ is the variance of the first mode shape resulting from the variability of source depth.

In (14), $\sigma_{\text{SL}} = 0.9$ and $\sigma_{\psi_1(z_0)}$ can be approximately estimated by calculating the variation of ψ_1 when the source depth varies between its upper (19.5 m) and lower (17.3 m) bound. Then, the only unknown in (14), σ_{β_1}, can be computed. Finally, the uncertainty of inverted mud attenuation due to σ_{SL} and $\sigma_{\psi_1(z_0)}$ is evaluated by taking the values of $(1.4737 \times 10^{-5} + \sigma_{\beta_1})$ dB/m and $(1.4737 \times 10^{-5} - \sigma_{\beta_1})$ dB/m as inputs for $\hat{\beta}_1$ to (9) and comparing the difference between the corresponding mud attenuations. The resulting uncertainty (0.004 dB/m) is on the same order of magnitude as the one (0.003 dB/m) caused by the modal amplitude measurement.

VI. Conclusion

Measured signals from long-range explosive sound sources were utilized to extract the acoustic normal mode characteristics including mode shape, modal dispersion curve, and modal amplitude. Modal characteristics of low-order modes were used in geoacoustic inversion algorithms to estimate low-frequency sound speed and attenuation in a surface mud layer, which overlaid three sand transition layers and a half-space basement. The properties in deeper layers inverted from the Airy phase structure [24] and the detailed environmental measurements from SBCEX 2017 as well as the bottom data (e.g., layer structure and density) from sediment surveys were applied as constraint conditions. It should be pointed out that the depth-dependent SSP (around 1.8 1/s) in the mud layer was obtained based on the assumption that a linear sound-speed gradient exists. If a different assumption (e.g., parabolic and decrease with depth) is adopted, the resulting SSP could be different. In this paper, we also assume that the sound speed in the mud layer is frequency independent in the band of 100–500 Hz. The sound speed dispersion will be examined in our future study.

Regarding the resolution (in depth) of the sound-speed inversion, the resolution length provides the minimum layer thickness that can be estimated based on the information content in the data. In the inversion approach presented in this paper, the resolution length is dependent on frequency, mode number, and depth. Generally, high-frequency data corresponding to a short wavelength will result in a small resolution length. For a fixed frequency (i.e., 150 Hz) and depth (i.e., surface mud layer), Fig. 7(b) and (c) shows that the variation of the first mode shape is smaller than that of the third mode. This indicates that the resolution length varies as mode number changes. The depth dependence has been discussed by Lin *et al.* [54] and Wan *et al.* [24]. In this paper, the first mode at 150 Hz mainly traveled in the water column and the surface mud layer, it was more sensitive to the geoacoustic parameters in the mud layer than those in the deeper layers. Therefore, the resolution length was smaller in mud. The dimension reduction was achieved by taking advantage of this depth dependence of the resolution length. A detailed quantitative study on the resolution length will be one of our future research tasks.

According to (8), an overestimated attenuation in sand will cause an underestimated attenuation in mud. The inversion of low-frequency attenuation in the surface mud layer is challenging because of this ambiguity between attenuation in mud and sand. As we showed in the previous sections, the normalized amplitudes of the first mode, ψ_1, at 150 Hz in the layers beneath the mud were small and β_1 was not sensitive to the geoacoustic parameters in these layers. Thus, the ambiguity was approximately removed. It is noted that the estimated attenuation value in the mud layer is based on the assumption of its depth and range independence, therefore it is the averaged value over the mud layer thickness and over the long propagation distance.

Based on the low-order modes, this inversion method with a dimension-reduced parameter space could provide a more effective way to obtain reliable estimates of mud properties compared with full field inversion methods. Furthermore, the geoacoustic properties of the surface mud layer determined by low-order modes could be used as constraints in a full field inversion approach to explore the properties in the deeper layers.

Acknowledgment

The authors would like to thank G. Schoch and C. Dixon from the Naval Surface Warfare Center for the operation of the explosive charges. The efforts of all the SBCEX 2017 participants are gratefully acknowledged. The authors would also like to thank the anonymous reviewers for their valuable suggestions and comments on the earlier version of this paper.

REFERENCES

[1] R. L. Folk, *Petrology of Sedimentary Rocks.* Austin, TX, USA: Hemphill Publishing Company, 1980, p. 26.

[2] E. L. Hamilton, "Geoacoustic modeling of the sea floor," *J. Acoust. Soc. Amer.*, vol. 68, no. 5, pp. 1313–1339, 1980.

[3] D. R. Jackson and M. D. Richardson, *High-Frequency Seafloor Acoustics.* New York, NY, USA: Springer, 2006, pp. 30–32.

[4] N. P. Chotiros, *Acoustics of the Seabed as a Poroelastic Medium.* Cham, Switzerland: Springer, 2017, pp. 3–5.

[5] M. Badiey, A. H.-D. Cheng, and Y. Mu, "From geology to geoacoustics—Evaluation of Biot–Stoll sound speed and attenuation for shallow water acoustics," *J. Acoust. Soc. Amer.*, vol. 103, no. 1, pp. 309–320, 1998.

[6] P. S. Wilson and D. P. Knobles, "An overview of the seabed characterization experiment," *J. Acoust. Soc. Amer.*, vol. 142, no. 4, p. 2556, 2017.

[7] D. C. Twichell, C. E. McClennen, and B. Butman, "Morphology and process associated with the accumulation of the fine-grained sediment deposit on the southern New England Shelf," *J. Sedimentary Petrology*, vol. 51, no. 1, pp. 0269–0280, 1981.

[8] M. H. Bothner, E. C. Spiker, P. P. Johnson, R. R. Rendigs, and P. J. Aruscavage, "Geochemical evidence for modern sediment accumulation on the continental shelf off southern New England," *J. Sedimentary Petrology*, vol. 51, no. 1, pp. 281–292, 1981.

[9] J. D. Chaytor, "Measurements of geologic characteristics, geophysical properties, and geoacoustic response of sediments from the New England Mud Patch," presented at the ONR Seabed Characterization Experiment Workshop VI, Seattle, WA, USA, May 30–31, 2017.

[10] F. Ingenito, "Measurement of mode attenuation coefficients in shallow water," *J. Acoust. Soc. Amer.*, vol. 53, no. 3, pp. 858–863, 1973.

[11] C. T. Tindle, "Attenuation parameters from normal mode measurements," *J. Acoust. Soc. Amer.*, vol. 71, no. 5, pp. 1145–1148, 1982.

[12] J. X. Zhou, "Normal mode measurements and remote sensing of seabottom sound velocity and attenuation in shallow water," *J. Acoust. Soc. Amer.*, vol. 78, no. 3, pp. 1003–1009, 1985.

[13] J. X. Zhou, X. Z. Zhang, P. H. Rogers, and J. Jarzynski, "Geoacoustic parameters in a stratified sea bottom from shallow-water acoustic propagation," *J. Acoust. Soc. Amer.*, vol. 82, no. 6, pp. 2068–2074, 1987.

[14] M. Badiey, I. Jaya, and A. H.-D. Cheng, "Shallow-water acoustic/geoacoustic experiments at the New Jersey Atlantic Generating Station site," *J. Acoust. Soc. Amer.*, vol. 96, no. 6, pp. 3593–3604, 1994.

[15] G. R. Potty, J. H. Miller, J. F. Lynch, and K. F. Smith, "Tomographic inversion for sediment parameters in shallow water," *J. Acoust. Soc. Amer.*, vol. 108, no. 3, pp. 973–986, 2000.

[16] P. Hursky, W. S. Hodgkiss, and W. A. Kuperman, "Matched field processing with data-derived modes," *J. Acoust. Soc. Amer.*, vol. 109, no. 4, pp. 1355–1366, 2001.

[17] G. R. Potty, J. H. Miller, and J. F. Lynch, "Inversion for sediment geoacoustic properties at the New England Bight," *J. Acoust. Soc. Amer.*, vol. 114, no. 4, pp. 1874–1887, 2003.

[18] Z. L. Li and R. H. Zhang, "Geoacoustic inversion based on dispersion characteristic of normal modes in shallow water," *Chin. Phys. Lett.*, vol. 24, no. 2, pp. 471–474, 2007.

[19] L. Wan, J. X. Zhou, and P. H. Rogers, "Low frequency sound speed and attenuation in sandy seabottom from long-range broadband acoustic measurements," *J. Acoust. Soc. Amer.*, vol. 128, no. 2, pp. 578–589, 2010.

[20] S. Rajan and K. M. Becker, "Inversion for range-dependent sediment compressional-wave-speed profiles from modal dispersion data," *IEEE J. Ocean. Eng.*, vol. 35, no. 1, pp. 43–58, Jan. 2010.

[21] J. Bonnel and N. R. Chapman, "Geoacoustic inversion in a dispersive waveguide using warping operators," *J. Acoust. Soc. Amer.*, vol. 130, no. 2, pp. EL101–EL107, 2011.

[22] Z. H. Michalopoulou and A. Pole, "Sediment sound speed inversion with time-frequency analysis and modal arrival time probability density functions," *J. Acoust. Soc. Amer.*, vol. 140, no. 1, pp. EL131–EL136, 2016.

[23] L. Wan, M. Badiey, and D. P. Knobles, "Geoacoustic inversion using low frequency broadband acoustic measurements from L-shaped arrays in the Shallow Water 2006 Experiment," *J. Acoust. Soc. Amer.*, vol. 140, no. 4, pp. 2358–2373, 2016.

[24] L. Wan, M. Badiey, D. P. Knobles, and P. S. Wilson, "The Airy phase of explosive sounds in shallow water," *J. Acoust. Soc. Amer.*, vol. 143, no. 3, pp. EL199–EL205, 2018.

[25] J. Bonnel *et al.*, "Geoacoustic inversion on the New England Mud Patch using warping and dispersion curves of high-order modes," *J. Acoust. Soc. Amer.*, vol. 143, no. 5, pp. EL405–EL411, 2018.

[26] A. Tolstoy, *Matched Field Processing for Underwater Acoustics.* Singapore: World Scientific, 1993.

[27] S. E. Dosso, M. L. Yeremey, J. M. Ozard, and N. R. Chapman, "Estimation of ocean-bottom properties by matched field inversions of acoustic field data," *IEEE J. Ocean. Eng.*, vol. 18, no. 3, pp. 232–239, Jul. 1993.

[28] P. Gerstoft, "Inversion of seismoacoustic data using genetic algorithms and a posteriori probability distributions," *J. Acoust. Soc. Amer.*, vol. 95, no. 2, pp. 770–782, 1994.

[29] S. D. Rajan, "Waveform inversion for the geoacoustic parameters of the ocean bottom," *J. Acoust. Soc. Amer.*, vol. 91, no. 6, pp. 3228–3241, 1992.

[30] D. P. Knobles, R. A. Koch, L. A. Thompson, and K. C. Focke, "Sound propagation in shallow water and geoacoustic inversion," *J. Acoust. Soc. Amer.*, vol. 113, no. 1, pp. 205–222, 2003.

[31] D. P. Knobles, T. W. Yudichak, R. A. Koch, P. G. Cable, J. H. Miller, and G. R. Potty, "Inferences on seabed acoustics in the East China Sea from distributed acoustic measurements," *IEEE J. Ocean. Eng.*, vol. 31, no. 1, pp. 129–144, Jan. 2006.

[32] D. P. Knobles *et al.*, "Maximum entropy derived statistics of sound speed structure in a fine-grained sediment inferred from sparse broadband acoustic measurements on the New England continental shelf," *IEEE J. Ocean. Eng.*, to be published.

[33] I. Rozenfeld, W. M. Carey, P. G. Cable, and W. L. Siegmann, "Modeling and analysis of sound transmission in the Strait of Korea," *IEEE J. Oceanic Eng.*, vol. 26, no. 4, pp. 809–820, Oct. 2001.

[34] S. M. Dediu, W. L. Siegmann, and W. M. Carey, "Statistical analysis of sound transmission results on the New Jersey continental shelf," *J. Acoust. Soc. Amer.*, vol. 122, no. 2, pp. EL23–EL28, 2007.

[35] J. X. Zhou *et al.*, "Reverberation vertical coherence and sea-bottom geoacoustic inversion in shallow water," *IEEE J. Ocean. Eng.*, vol. 29, no. 4, pp. 988–999, Oct. 2004.

[36] M. Buckingham and S. Jones, "A new shallow ocean technique for determining the critical angle of the seabed from the vertical directionality of the ambient noise in the water column," *J. Acoust. Soc. Amer.*, vol. 81, no. 4, pp. 938–946, 1987.

[37] N. M. Carbon, G. B. Deane, and M. J. Buckingham, "Estimating the compressional and shear wave speeds of a shallow water seabed from the vertical coherence of ambient noise in the water column," *J. Acoust. Soc. Amer.*, vol. 103, no. 2, pp. 801–813, 1998.

[38] C. W. Holland, "Seabed reflection measurement uncertainty," *J. Acoust. Soc. Amer.*, vol. 114, no. 4, pp. 1861–1873, 2003.

[39] J. Dettmer, S. E. Dosso, and C. W. Holland, "Full wave-field reflection coefficient inversion," *J. Acoust. Soc. Amer.*, vol. 122, no. 6, pp. 3327–3337, 2007.

[40] G. V. Frisk and J. F. Lynch, "Shallow water waveguide characterization using the Hankel transform," *J. Acoust. Soc. Amer.*, vol. 76, no. 1, pp. 205–216, 1984.

[41] K. M. Becker, S. D. Rajan, and G. V. Frisk, "Results from the geoacoustic inversion techniques workshop using modal inverse methods," *IEEE J. Ocean. Eng.*, vol. 28, no. 3, pp. 331–341, Jul. 2003.

[42] Y. M. Jiang, N. R. Chapman, and P. Gerstoft, "Short range travel time geoacoustic inversion with vertical line array," *J. Acoust. Soc. Amer.*, vol. 124, no. 3, pp. EL135–EL140, 2008.

[43] J. X. Zhou, X. Z. Zhang, and D. P. Knobles, "Low-frequency geoacoustic model for the effective properties of sandy seabottoms," *J. Acoust. Soc. Amer.*, vol. 125, no. 5, pp. 2847–2866, 2009.

[44] J. C. Papp, J. C. Preisig, and A. K. Morozov, "Physically constrained maximum likelihood mode filtering," *J. Acoust. Soc. Amer.*, vol. 127, no. 4, pp. 2385–2391, 2010.

[45] D. M. Milder, "Ray and wave invariants for SOFAR channel propagation," *J. Acoust. Soc. Amer.*, vol. 46, no. 5, pp. 1259–1263, 1969.

[46] J. A. Goff, J. D. Chaytor, A. H. Reed, S. H. Liu, P. S. Wilson, and D. P. Knobles, "The coarse- to fine-grained boundary beneath the New England Mud Patch: Evidence from seismic and core data for an abrupt post-transgressive change in hydrologic regime on the continental shelf," presented at the Amer. Geophys. Union Fall Meeting, San Francisco, CA, USA, December 12–16, 2016.

[47] J. A. Goff, A. H. Reed, G. Gawarkiewicz, P. S. Wilson, and D. P. Knobles, "Stratigraphic analysis of a sediment pond within the southern New England Mud Patch: New constraints from high-resolution chirp acoustic reflection data," *Mar. Geol.*, vol. 412, pp. 81–94, 2019.

[48] A. Reed and E. Braithwaite, "P-wave velocity and density: Core logging," presented at the ONR Seabed Characterization Experiment Workshop IV, Arlington, VA, USA, Jun. 6–8, 2016.

[49] M. Zeh, A. R. McNeese, P. S. Wilson, and D. P. Knobles, "Source characteristics of small explosive charges in shallow water," *IEEE J. Ocean. Eng.*, to be published.

[50] M. B. Porter, "The KRAKEN normal mode program," SACLANT Undersea Res. Centre, La Spezia, Italy, Rep. SM-245, 1991.

[51] R. A. Koch, C. Penland, P. J. Vidmar, and K. E. Hawker, "On the calculation of normal mode group velocity and attenuation," *J. Acoust. Soc. Amer.*, vol. 73, no. 3, pp. 820–825, 1983.
[52] F. B. Jensen, W. A. Kuperman, M. B. Porter, and H. Schmidt, *Computational Ocean Acoustics.* New York, NY, USA: Springer, 2011, pp. 36–38.
[53] J. R. Taylor, *An Introduction to Error Analysis.* Sausalito, CA, USA: Univ. Sci. Books, 1997, pp. 186–192.
[54] Y.-T. Lin *et al.*, "An estimate of the bottom compressional wave speed profile in the northeastern south China Sea using sources of opportunity," *IEEE J. Ocean. Eng.*, vol. 29, no. 4, pp. 1231–1248, Oct. 2004.

Lin Wan received the double B.S. degrees in mechanical engineering and electrical and electronics engineering and the M.S. degree in ocean acoustics from Shanghai Jiao Tong University, Shanghai, China, in 2000 and 2003, respectively. He received the M.S. degree in industrial engineering and the Ph.D. degree in mechanical engineering from Georgia Institute of Technology (Georgia Tech), Atlanta, GA, USA, in 2008 and 2010, respectively.

He worked as a Postdoctoral Fellow with the School of Mechanical Engineering at Georgia Tech. After his postdoctoral research at Georgia Tech, he joined the Ocean Acoustics Laboratory at University of Delaware, Newark, DE, USA, where he is currently a Research Faculty with the Electrical and Computer Engineering Department. He has been conducting experimental and theoretical research in ocean acoustics, acoustical oceanography, and acoustic signal processing. He is the Principal Investigator of an Office of Naval Research (ONR) grant to study the geoacoustic properties in muddy sediments using broadband acoustic signals. His research interests include geoacoustic inversion, internal wave effects on three-dimensional sound propagation in shallow water, and Arctic acoustics.

Dr. Wan was a recipient of the U.S. Navy ONR Graduate Traineeship Award supported by the special research award from the Ocean Acoustics program. He is a member of the Acoustical Society of America.

Mohsen Badiey received the Ph.D. degree in applied marine physics and ocean engineering from Rosenstiel School of Marine and Atmospheric Science, University of Miami, Coral Gables, FL, USA, in 1988.

From 1988 through 1990, he was a Postdoctoral Fellow with the Port and Harbor Research Institute, Ministry of Transport in Japan. After his postdoctoral research, he became a faculty member with the University of Delaware, Newark, DE, USA, where he is currently a Professor. From 1992 to1995, he was a Program Director and Scientific Officer with the Office of Naval Research, where he served as the team leader to formulate long-term naval research in the field of acoustical oceanography. His research interests are physics of sound and vibration, shallow water acoustics and oceanography, underwater acoustic communications, seabed acoustics, and geophysics.

Dr. Badiey is a Fellow of the Acoustical Society of America.

David P. Knobles received the Ph.D. degree in nuclear theory from the University of Texas at Austin, Austin, TX, USA, in 1989.

From 1989 through 1992, he did a postdoctoral fellowship in nuclear physics at the University of Texas at Austin. He was a Research Scientist with The Applied Research Laboratories, The University of Texas at Austin, in 1980–1985 and 1992–2016. He is currently the owner of Knobles Scientific and Analysis, a private business that specializes in defense and environmental applications. He has been a Principle Investigator in the Ocean Acoustics Program with the Office of Naval Research since 2002. He has taught graduate courses at the University of Texas at Austin in methods of mathematical physics and ocean acoustics. His research interests include theoretical physics, remote sensing, cosmology, and bioacoustics.

Dr. Knobles is currently serving as a Co-Chief Scientist for the ONR Seabed Characterization Experiment. He is a Fellow of the Acoustical Society of America.

Preston S. Wilson received the B.S. and M.S. degrees in mechanical engineering from The University of Texas at Austin, Austin, TX, USA, in 1990 and 1994, respectively, and the Ph.D. degree in mechanical engineering from Boston University, Boston, MA, USA, in 2001.

He is currently a Professor and Raymond F. Dawson Centennial Fellow in engineering with the University of Texas at Austin, Austin, TX, USA, with joint appointments in the Mechanical Engineering Department and Applied Research Laboratories (ARL:UT). He was a Research Engineer with ARL:UT from 1993 through 1997, served as a Postdoctoral Fellow with Boston University, from 2001 to 2003, and has been a Faculty Member with University of Texas at Austin since 2003. His work has been reported in more than 360 peer reviewed papers, conference proceedings, technical reports, and published presentation abstracts. He holds six U.S. patents, and is a Co-Founder of AdBm, Inc., operating in the underwater noise mitigation arena. His research areas are broadly focused on physical acoustics, underwater acoustics, engineering acoustics, and bioacoustics, with specific areas of interest in sound propagation in shallow water, in watersaturated sediments, bubbly liquid, and multiphase material.

Dr. Wilson is a Fellow of the Acoustical Society of America (ASA), the Past-Chair of the Committee for Education in Acoustics of the ASA, a current member of the Executive Council of the ASA, and an Associate Editor of the *Journal of the Acoustical Society of America*. He is currently serving as a Co-Chief Scientist for the ONR Seabed Characterization Experiment. He was the recipient of the A.B. Wood Medal from the Institute of Acoustics U.K.

John A. Goff received an Sc.B. degree in geophysics-math from Brown University in 1985, and a Ph.D. degree in oceanography from the MIT/Woods Hole Oceanographic Institution Joint Program in 1990.

After two years of postdoc work at the Woods Hole Oceanographic Institution, he began work as an Associate Research Scientist at the University of Texas Institute for Geophysics in 1993, where he has remained ever since. He was promoted to Research Scientist in 1999, and Senior Research Scientist in 2004. He served as associate editor for the Journal of Geophysical Research from 1995 to 1997, and as the Earth Processes/Tectonophysics and Seismology editor for Eos from 1999 to 2003. He is a member of the Society of Exploration Geophysicists and the American Geophysical Union. His research involves seafloor mapping, subseafloor imaging and sediment characterization in near-shore and continental shelf settings, as well as stochastic modeling of a variety of geophysical fields.